Catalytic Oxidation of NO over LaCo₁₋ₓBₓO₃ (B = Mn, Ni) Perovskites for Nitric Acid Production

Ata ul Rauf Salman [1] [iD], **Signe Marit Hyrve** [1], **Samuel Konrad Regli** [1] [iD], **Muhammad Zubair** [1], **Bjørn Christian Enger** [2], **Rune Lødeng** [2], **David Waller** [3] [iD] **and Magnus Rønning** [1,*] [iD]

[1] Department of Chemical Engineering, Norwegian University of Science and Technology (NTNU), Sem Sælands vei 4, NO-7491 Trondheim, Norway; ata.r.salman@ntnu.no (A.u.R.S.); signemhyrve@gmail.com (S.M.H.); samuel.k.regli@ntnu.no (S.K.R.); muhammad.zubair@ntnu.no (M.Z.)

[2] SINTEF Industry, Kinetic and Catalysis Group, P.O. Box 4760 Torgarden, NO-7465 Trondheim, Norway; bjorn.christian.enger@sintef.no (B.C.E.); rune.lodeng@sintef.no (R.L.)

[3] YARA Technology Center, Herøya Forskningspark, Bygg 92, Hydrovegen 67, NO-3936 Porsgrunn, Norway; david.waller@yara.com

* Correspondence: magnus.ronning@ntnu.no; Tel.: +47-73594121

check for updates

Abstract: Nitric acid (HNO_3) is an important building block in the chemical industry. Industrial production takes place via the Ostwald process, where oxidation of NO to NO_2 is one of the three chemical steps. The reaction is carried out as a homogeneous gas phase reaction. Introducing a catalyst for this reaction can lead to significant process intensification. A series of $LaCo_{1-x}Mn_xO_3$ (x = 0, 0.25, 0.5 and 1) and $LaCo_{1-y}Ni_yO_3$ (y = 0, 0.25, 0.50, 0.75 and 1) were synthesized by a sol-gel method and characterized using N_2 adsorption, ex situ XRD, in situ XRD, SEM and TPR. All samples had low surface areas; between 8 and 12 m^2/g. The formation of perovskites was confirmed by XRD. The crystallite size decreased linearly with the degree of substitution of Mn/Ni for partially doped samples. NO oxidation activity was tested using a feed (10% NO and 6% O_2) that partly simulated nitric acid plant conditions. Amongst the undoped perovskites, $LaCoO_3$ had the highest activity; with a conversion level of 24.9% at 350 °C; followed by $LaNiO_3$ and $LaMnO_3$. Substitution of $LaCoO_3$ with 25% mol % Ni or Mn was found to be the optimum degree of substitution leading to an enhanced NO oxidation activity. The results showed that perovskites are promising catalysts for NO oxidation at industrial conditions.

Keywords: NO oxidation; catalytic oxidation; nitric oxide; perovskite; nitric acid; ostwald's process; in situ; $LaCoO_3$; $LaMnO_3$; $LaNiO_3$

1. Introduction

Oxidation of nitric oxide (Equation (1)) is one of the few known third order reactions. The reaction is unusual, as the rate of reaction increases with a decrease in the temperature [1]

$$2NO + O_2 \leftrightarrows NO_2 \qquad \Delta_r H_{298} = -113.8 \text{ kJ/mol} \qquad (1)$$
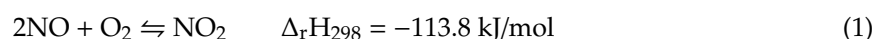
NO oxidation is a key reaction in lean NO_x abatement technologies and in the Ostwald process for nitric acid production. In Ostwald's process, NO oxidation is carried out as a non-catalytic process and the forward reaction is favored by the removal of heat and by providing sufficient residence time. Typical gas stream concentrations are 10% NO, 6% O_2 and 15% H_2O [2]. Using a catalyst for NO oxidation may lead to significant process intensification of the nitric acid plant. In addition to speeding up the oxidation process, it may reduce capital costs and increase heat recovery. Efforts have been made to find a catalyst effective under industrial conditions; but success so far has not been

achieved [2]. To date, the process is carried out as a homogenous process in modern nitric acid plants. To the best of the authors knowledge, apart from an earlier patent [3], only two recent studies [4,5] report catalytic oxidation of NO at nitric acid plant conditions. However, catalytic oxidation of NO has been extensively studied with regards to lean NO_x abatement technologies and reviewed by Russel and Epling [6] and Hong et al. [7]. In these studies, oxidation of NO is carried out at very lean concentrations of NO ranging from 100–1000 ppm of NO [8–10]. The huge difference in NO concentration between NO_x abatement and nitric acid production makes the extrapolation of these findings to nitric acid plant conditions, questionable.

Although it has been demonstrated that platinum has significant catalytic activity for oxidation of NO to NO_2 at nitric acid plant conditions [4,5] the high-cost and scarcity of platinum motivates the search for potential non-noble metal based catalysts.

Perovskites have gained particular interest as catalytic materials due to their high thermal stability, ease of synthesis and good catalytic activity [11]. Perovskites are represented by a general formula ABO_3, where A represents a rare earth or alkaline earth cation and B represents a transition metal cation. The activity of perovskites can be tuned by partial substitution of A and/or B site cations with another element to obtain the desired properties [11]. The lanthanum-based perovskite *$LaBO_3$* (B = Co, Mn, Ni) have been found to be active for NO oxidation at lean NO conditions [12,13]. It has been demonstrated for $LaCoO_3$, that partial doping of the A-site with strontium or cerium or doping of the B-site with manganese or nickel enhances NO oxidation activity of the perovskite [13–16].

In this work, lanthanum-based perovskites with cobalt, nickel and manganese ($LaCoO_3$, $LaNiO_3$ and $LaMnO_3$) were synthesized by the sol-gel method using citric acid. Catalytic tests were performed using a dry feed (10% NO, 6% O_2) at atmospheric pressure; partially simulating nitric acid plant conditions. The effect of B-site substitution was studied by preparing a series of $LaCo_{1-x}Mn_xO_3$ and $LaCo_{1-y}Ni_yO_3$ catalysts. The catalysts were characterized using N_2 adsorption, X-ray diffraction (XRD), Scanning electron microscopy (SEM) and temperature programmed reduction (TPR). Catalyst structure during pretreatment and oxidation of NO was monitored using in situ XRD.

2. Results and Discussion

2.1. Catalyst Characterisation

Specific surface areas are summarized in Table 1. All samples have a relatively low surface area, in the range of 8–12 m^2/g, which is a typical of perovskites prepared by the citrate method [14,17,18]. The surface area remains unaffected by the degree of substitution of Mn (x). However, an irregular change in surface area is observed with the degree of substitution of Ni (y). For $y = 0.25$ and 0.75, the surface area increased by 25% (from 8 to 10 m^2/g) and 50% (from 8 to 12 m^2/g) respectively. However, for $y = 0.50$ the surface area remains the same as for $LaCoO_3$.

Table 1. Brunauer–Emmett–Teller (BET) surface area and crystallite size (d) calculated using the Scherrer equation.

Sample	Surface Area (m^2/g)	d (nm)
$LaCoO_3$	8	28
$LaCo_{0.75}Mn_{0.25}O_3$	8	24
$LaCo_{0.50}Mn_{0.50}O_3$	7	18
$LaMnO_3$	9	21
$LaCo_{0.75}Ni_{0.25}O_3$	10	22
$LaCo_{0.50}Ni_{0.50}O_3$	8	17
$LaCo_{0.25}Ni_{0.75}O_3$	12	8
$LaNiO_3$	8	13

The XRD patterns shown in Figure 1 reveal the formation of phase-pure perovskite structure for all samples, and no peaks characteristic of the metallic oxides or carbonates were seen. The main characteristic peak at $2\theta = 33°$ for $LaCoO_3$ slightly shifts towards lower 2θ values with an increase in x and y, indicating an increase in the lattice parameters confirming previous findings [13,19,20]. This expansion can be explained by comparing the ionic radii of the species in the perovskite structure. The higher ionic radii of Ni^{3+} (0.56 Å) than Co^{3+} (0.52 Å) responsible for lattice expansion in $LaCo_{1-y}Ni_yO_3$ [20]. In case of $LaCo_{1-x}Mn_xO_3$, the average trivalent metal site is conserved by adjusting the ratio between Mn^{4+}/Mn^{3+} and Co^{3+}/Co^{2+} [21]. Therefore, the relative amount of Mn^{4+} (0.52 Å) present, Mn^{3+} (0.645 Å), Co^{2+} (0.82 Å), Co^{3+} (0.52 Å) dictates the overall lattice parameters.
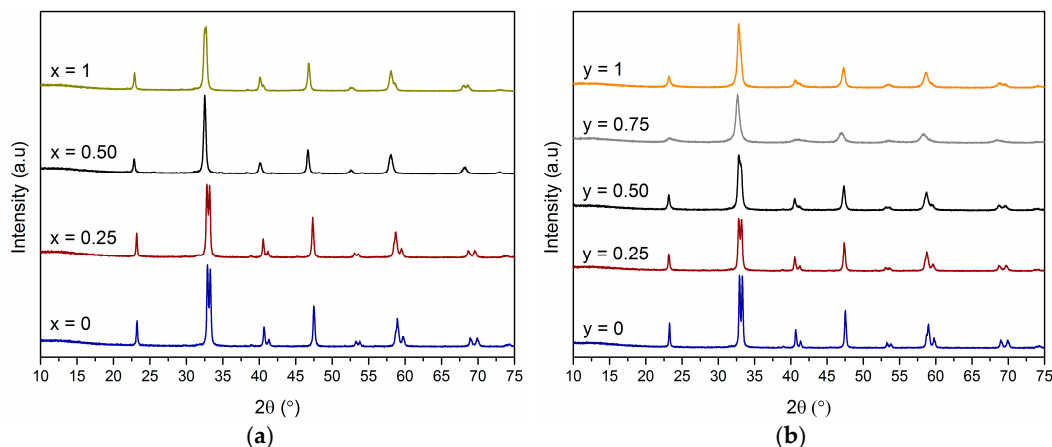

Figure 1. XRD patterns of: (**a**) $LaCo_{1-x}Mn_xO_3$; (**b**) $LaCo_{1-y}Ni_yO_3$ perovskites.

Among undoped perovskites, $LaCoO_3$ and $LaMnO_3$ belong to the rhombohedral phase in agreement with the results reported in literature [22,23]. $LaNiO_3$ belongs to the cubic phase, which is consistent with previous studies [24].

Crystallite sizes calculated using the Scherrer equation are summarized in Table 1. Figure 2 shows crystallite size as a function of the degree of substitution. The highest crystallite size of 28 nm was observed for $LaCoO_3$ and a linear decrease was observed with an increase in x and y for partially substituted samples indicating that partial substitution effectively restrains the crystal growth. However, other contributions to XRD peak broadening such as strain cannot be ruled out. Partially substituted nickel perovskites had smaller crystallite size compared to their manganese counterparts.
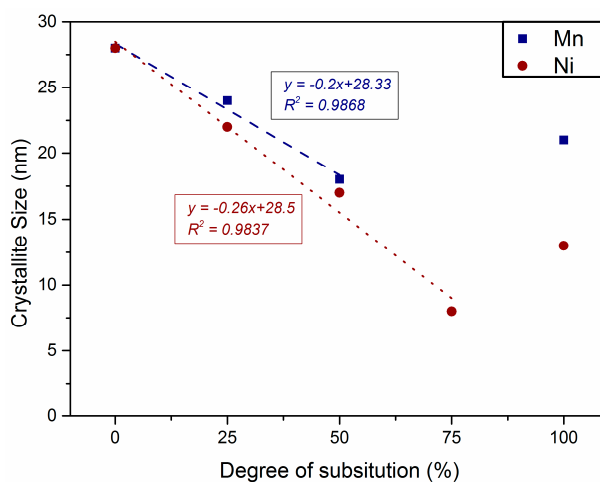

Figure 2. Crystallite size as a function of the degree of substitution for $LaCo_{1-x}Mn_xO_3$ and $LaCo_{1-y}Ni_yO_3$ perovskites.

Figure 3 shows the XRD pattern recorded in situ during pretreatment of $LaCoO_3$ and $LaMnO_3$. No change in structure is observed apart from lattice expansion with an increase in temperature. The structural stability of the perovskites is in accordance with the fact that they are calcined at higher temperatures in comparison with the pretreatment temperature of 500 °C. No change in structure was observed for $LaCoO_3$ and $LaMnO_3$ during steady state oxidation of NO at 350 °C indicating that the bulk structure of perovskite remains unaffected during the catalytic process. However, minor changes beyond the detectable range of XRD cannot be ruled out.
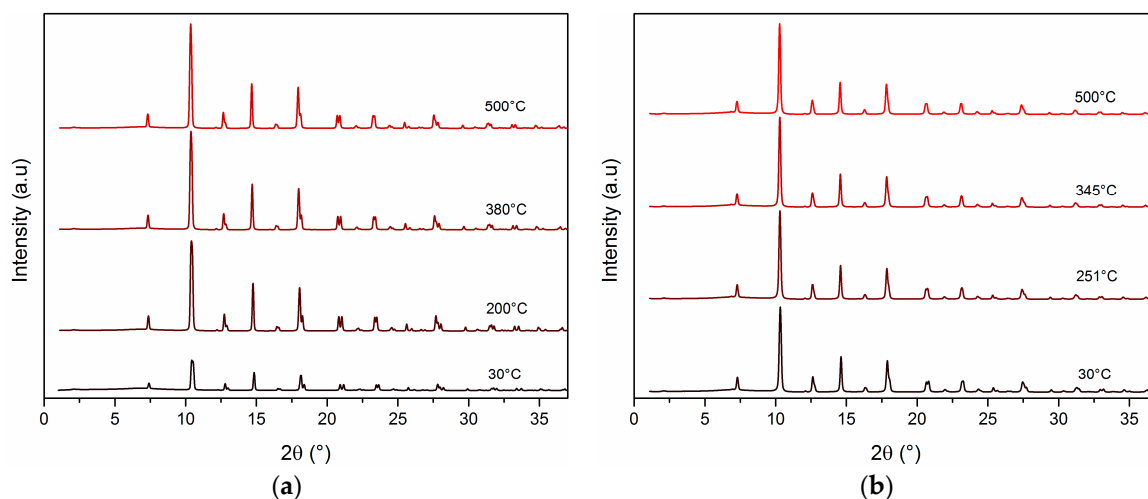

Figure 3. XRD patterns (λ = 0.49324 Å) recorded in situ during pretreatment of: (**a**) $LaCoO_3$; (**b**) $LaMnO_3$ perovskites.

Figure 4 shows the SEM images of $LaCoO_3$ with varying content of Mn and pure $LaNiO_3$. The presence of agglomerated non-spherical particles is observed for all samples. A significant change in morphology is observed with the substitution of Co with Mn along with an increase in the extent of agglomeration (Figure 4b–d).
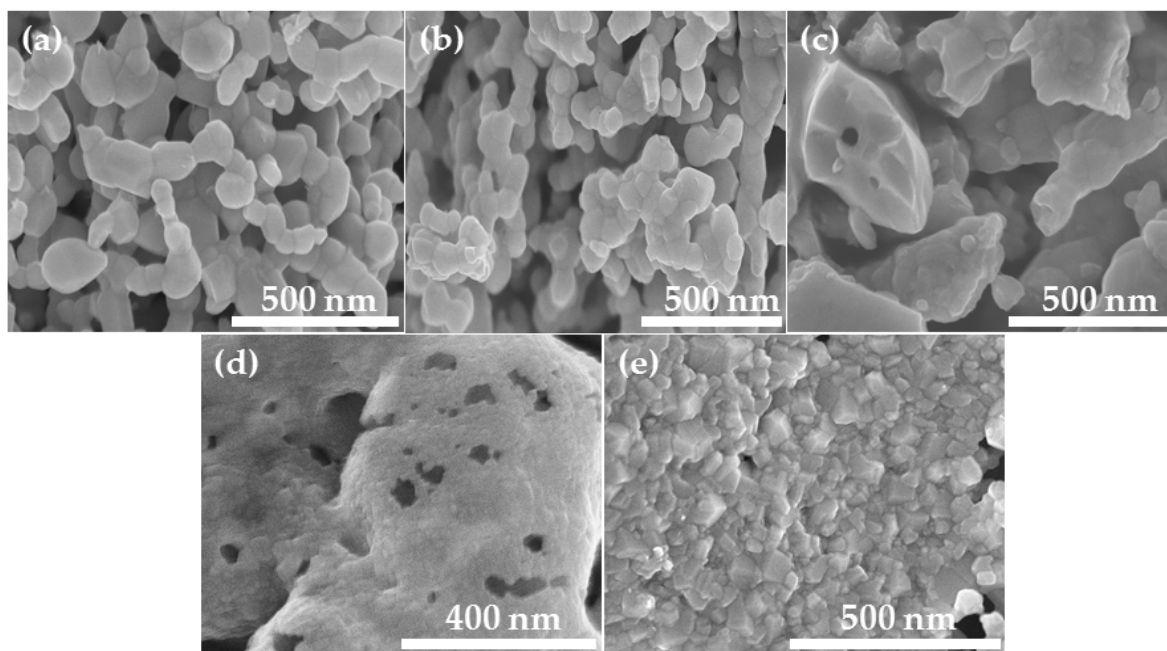

Figure 4. SEM images: (**a**) $LaCoO_3$; (**b**) $LaCo_{0.75}Mn_{0.25}O_3$; (**c**) $LaCo_{0.50}Mn_{0.50}O_3$; (**d**) $LaMnO_3$; (**e**) $LaNiO_3$.

The H_2-TPR profiles of $LaCo_{1-x}Mn_xO_3$ perovskites are given in Figure 5a. Three reduction peaks at 334, 373 and 526 °C are observed in the TPR profile of $LaCoO_3$. The first two peaks are attributed to the reduction of Co^{3+} to Co^{2+}, while the peak at 526 °C represents the reduction of Co^{2+} to Co^0 leading to the destruction of the perovskite structure [25]. TPR of $LaMnO_3$ shows two main reduction peaks at 383 and 818 °C. The first peak represents the reduction of Mn^{4+} to Mn^{3+}, while the reduction of Mn^{3+} to Mn^{2+} occurs at elevated temperatures (above 700 °C), forming MnO and simultaneous collapse of the perovskite structure [26]. For *x = 0.25* and *0.5*, broad peaks overlapping reduction peaks of Co^{3+} to Co^{2+} and Mn^{4+} to Mn^{3+} are observed below 550 °C.
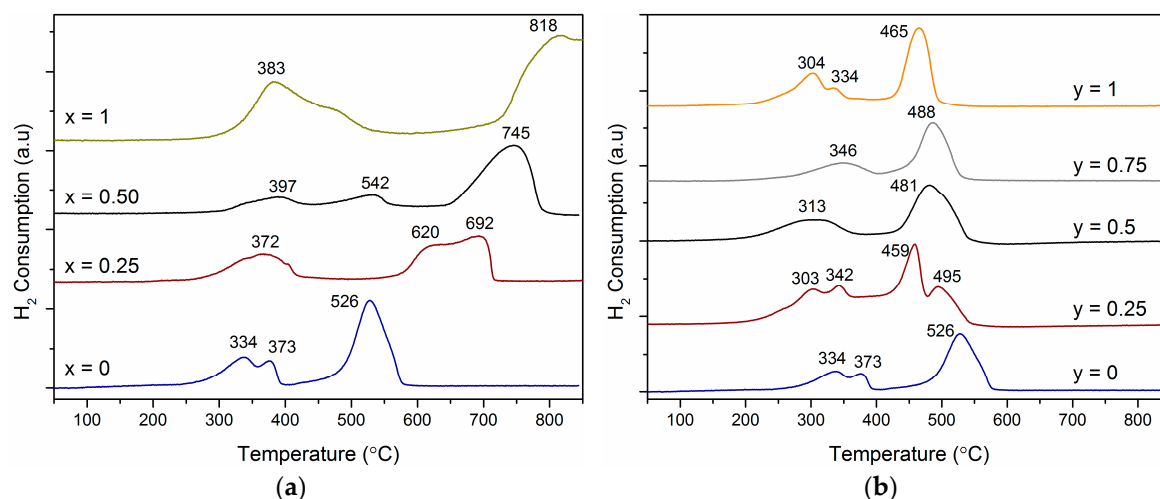
Figure 5. TPR profiles of: (**a**) $LaCo_{1-x}Mn_xO_3$; (**b**) $LaCo_{1-y}Ni_yO_3$ perovskites.

Figure 5b shows H_2-TPR profiles of $LaCo_{1-y}Ni_yO_3$ perovskites. Reduction of $LaNiO_3$ also proceeds via three peaks at 304 °C, one at 334 °C and one at 465 °C. A similar three-step reduction process for $LaNiO_3$ has been reported [27] and in situ XRD revealed that reduction proceeds via formation of the La_2NiO_4 phase [27]. The highest peak is associated with the formation of Ni^0 and La_2O_3 resulting in the destruction of the perovskite structure. Four reduction peaks were observed for *y = 0.25*. Comparison with $LaCoO_3$ and $LaNiO_3$ indicates that the first two peaks at 303 and 342 °C match with the reduction peaks of Ni^{3+} to Ni^{2+} and Co^{3+} to Co^{2+}. Whereas the former two peaks at 459, 495 °C corresponds to further reduction to form the metallic phases (Ni^0 and Co^0). This reduction profile matches well with the previous findings [20]. In contrast to distinct reduction peaks for cobalt and nickel for $LaCo_{0.75}Ni_{0.25}O_3$, only two broad peaks were observed for *y = 0.50* and *0.75*. The first peak overlaps with the reduction of Ni^{3+} to Ni^{2+} and Co^{3+} to Co^{2+} and increases from 313 °C for *y = 0.50* to 346 °C for *y = 0.75*. Simultaneous reduction to metallic phases (Ni^0 and Co^0) was observed at 418 °C and 488 °C for *y = 0.50* and *0.75*, respectively.

2.2. NO Oxidation Activity

The oxidation of NO occurs as a homogeneous gas-phase reaction with a second order dependency in NO concentration. For this reason, contributions from gas phase conversion have been detected for studies performed at lean NO concentrations [28–30]. This necessitates the quantification of the gas phase contribution to NO oxidation in the current study, which involves such a high concentration of NO (10%). The blank run performed without catalyst is given in our previous publication [5]. The gas phase conversion gradually decreases with increasing temperature in the studied temperature range (150–450 °C); with a conversion of 6.1% at 350 °C.

The conversion of NO over $LaCo_{1-x}Mn_xO_3$ as a function of temperature is shown in Figure 6. The NO conversion and rate of reaction are summarized in Table 2. At low temperature, only gas phase conversion is observed for all perovskites. The catalytic activity for $LaCoO_3$ starts at about 270 °C and

increases gradually until it becomes limited by the thermodynamic equilibrium. This is in contrast to studies performed at lean NO_x conditions, where the catalytic activity starts at significantly lower temperatures (150–200 °C); increases with a steeper slope, and becomes thermodynamically limited at ca 300 °C [14,15]. The catalytic conversion starts at a lower temperature (240 °C) for *x = 0.25* in comparison to other perovskites and a significant increase in conversion was observed. A further increase in *x* to *0.5* leads to a substantial decrease in NO conversion to conversion levels even lower than what is observed for $LaMnO_3$. Manganese is stable in valence states +III and +IV while cobalt is stable in valence states +II and +III. Ghiasi et al. [21] used X-ray absorption spectroscopy (XAS) to study the valence state of Mn and Co in a series of $LaCo_{1-x}Mn_xO_3$ perovskites and found that the average trivalent metal site is conserved by shifting the balance between Mn^{4+}/Mn^{3+} in combination with Co^{3+}/Co^{2+}. The ratio between Mn^{4+}/Mn^{3+} and Co^{3+}/Co^{2+} decreases with a sequential increase in manganese content, the highest value being observed for $LaCo_{0.75}Mn_{0.25}O_3$. The best activity of $LaCo_{0.75}Mn_{0.25}O_3$ in the series of $LaCo_{1-x}Mn_xO_3$ perovskites may be attributed to the presence of highest content of Mn^{4+} as amongst different valence states of manganese, Mn^{4+} (MnO_2) exhibits the highest activity for NO oxidation followed by Mn^{3+} (Mn_2O_3) and Mn^{2+} (Mn_3O_4) [31].
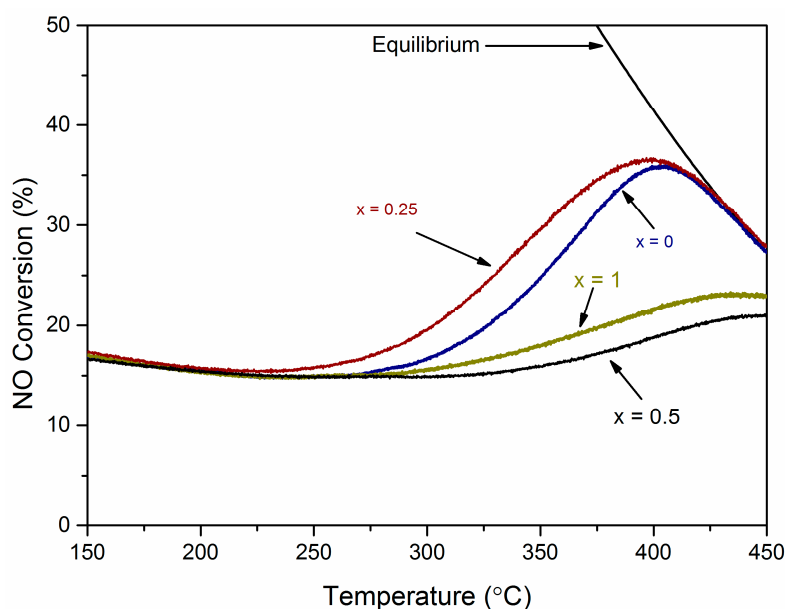

Figure 6. Conversion of NO over $LaCo_{1-x}Mn_xO_3$ as a function of temperature.

Table 2. NO oxidation activity of perovskites at 350 °C.

Sample	X_{NO} (%)	r_{NO} [1] ($\mu molg_{cat}^{-1}s^{-1}$)
$LaCoO_3$	24.9	5.14
$LaCo_{0.75}Mn_{0.25}O_3$	29.7	6.55
$LaCo_{0.50}Mn_{0.50}O_3$	15.9	2.72
$LaMnO_3$	18.0	3.27
$LaCo_{0.75}Ni_{0.25}O_3$	30.3	6.70
$LaCo_{0.50}Ni_{0.50}O_3$	23.2	4.74
$LaCo_{0.25}Ni_{0.75}O_3$	16.4	2.86
$LaNiO_3$	20.8	4.05

[1] Catalytic activity obtained by subtracting the gas phase conversion of NO.

Figure 7 shows the conversion of NO over $LaCo_{1-y}Ni_yO_3$ as a function of temperature. Minor difference in gas phase conversion is observed at lower temperatures due to the differences in the packing of the catalyst bed. The substitution with 25 mol% Ni in $LaCoO_3$ had a significant positive impact on the activity exhibiting a conversion of 30% at 350 °C. With a further increase in *y*, the activity

gradually decreased until 75% nickel content. Similar conversion curves are exhibited by *y = 0.5* and *y = 1* perovskites. Although our results differ from Zhong et al. [13], who reported 70 mol% nickel substitution in $LaCoO_3$ to yield the best results for NO oxidation, it can be argued that they used a co-precipitation method for preparation of perovskites and the activity was tested at substantially different feed concentration (400 ppm NO and 6% O_2) compared to the present study. The increase in activity for $LaCo_{0.75}Ni_{0.25}O_3$ can in part be attributed to the 25% increase in surface area. However, for $LaCo_{0.25}Ni_{0.75}O_3$ the surface area increased with 50% compared to $LaCoO_3$ and 33% compared to $LaNiO_3$, while the catalytic activity decreased. Thus, it seems likely that the change in catalytic activity is more related to the chemical oxygen dynamics and to the redox properties than to changes in the surface area in this range. Ivanova et al. [32] reported a maximum in defect structures for *x = 0.25* in a series of $LaCo_{1-x}Ni_xO_3$, detected by EPR due to the presence of magnetic Ni clusters. However, this depends on the method of preparation and pre-treatment procedure. The highest activity of $LaCo_{0.75}Ni_{0.25}O_3$ may thus be related to lattice defects not detectable by bulk XRD. The NO oxidation activity follows the order $LaCoO_3$ > $LaNiO_3$ > $LaMnO_3$ for the undoped perovskites.

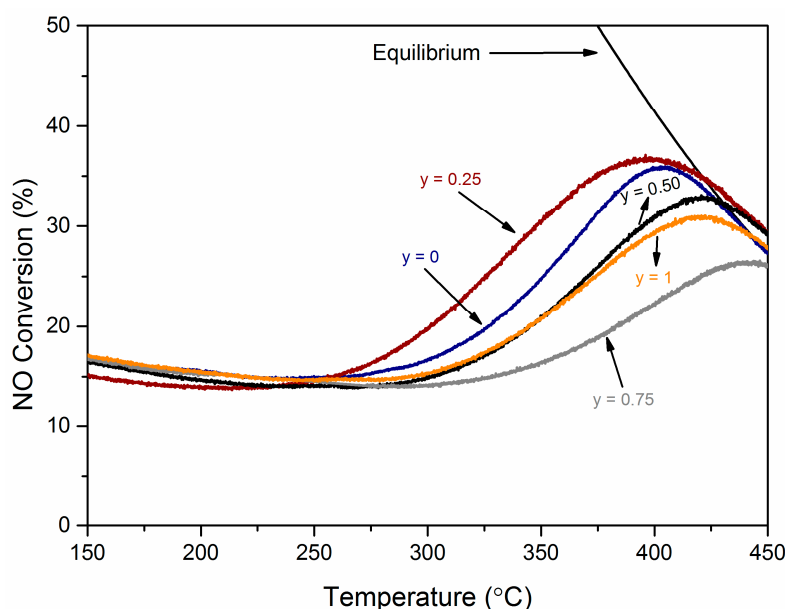**Figure 7.** Conversion of NO over $LaCo_{1-y}Ni_yO_3$ as a function of temperate.

Figure 8 shows the rate of reaction as a function of crystallite size for $LaCo_{1-x}Mn_xO_3$ and $LaCo_{1-y}Ni_xO_3$ perovskites. The rate of reaction increases linearly with crystallite size with *x = 0.25* and *y = 0.25* samples being the exception and not included in the linear fit. It should be kept in mind that the crystallite sizes were calculated using the Scherrer equation assuming spherical geometry. Though, the crystallites are not spherical as revealed through SEM images. The crystallite size estimates from the Scherrer equation might not be 100% accurate but they provide a fair comparison.

Partial substitution of $LaCoO_3$ with either manganese or nickel leads to a modification in the redox properties, morphology, structure, crystallite size and valence state of the metal site. Therefore, it is difficult to pinpoint one governing factor determining the catalytic activity. In fact, it is a combination of several factors which contribute to dictating catalytic activity.
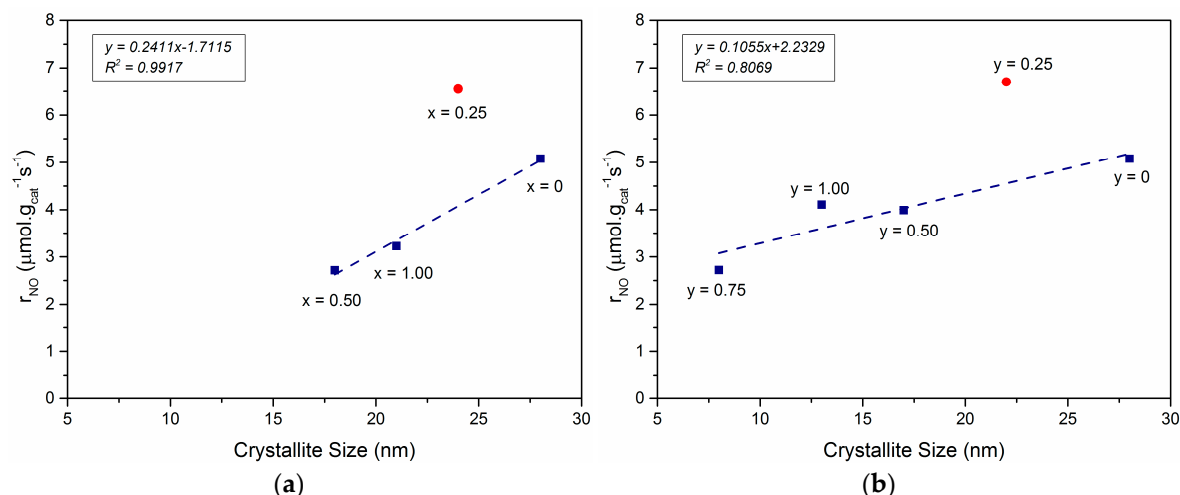
Figure 8. Rate of reaction as a function of crystallite size: (**a**) $LaCo_{1-x}Mn_xO_3$; (**b**) $LaCo_{1-y}Ni_yO_3$ perovskites.

3. Materials and Methods

3.1. Catalyst Preparation

All catalysts were prepared using the citrate method [14]. Nitrate salts were used as starting materials: $La(NO_3)_3 \cdot 6H_2O$ (Alfa Aesar, 99.9%, Kandel, Germany), $Mn(NO_3)_2 \cdot 4H_2O$ (Alfa Aesar, 99.98%, Kandel, Germany), $Co(NO_3)_3 \cdot 6H_2O$ (Acros Organics, 99%, Geel, Belgium) and $Ni(NO_3)_2 \cdot 6H_2O$ (Acros Organics, 99%, Geel, Belgium). An appropriate amount of nitrate salts of the desired A and B sites were dissolved in deionized water with 10 wt.% excess citric acid (Sigma Aldrich, 99.5%, Munich, Germany). The solution was stirred for 1 h at room temperature and further stirred in an oil bath at 80 °C until a viscous gel was obtained. The gel was dried in static air overnight at 90 °C and then heated to 150 °C for 1 h. The black, spongy material was crushed and calcined at 700 °C for 5 h in static air.

3.2. Catalyst Characterisation

N_2 adsorption was used to measure the specific surface area. The sample (200 mg) was degassed at 200 °C overnight in VacPrep 061 Degasser (Norcross, GA, USA). Nitrogen adsorption was performed with a Miromeritics TriStar II 3020 Surface Area and Porosity Analyzer (Norcross, GA, USA) at −196 °C. The specific surface areas were calculated using the BET desorption branch of the isotherm [33].

Ex situ XRD patterns of as prepared samples were obtained with a Bruker D8 Advanced X-ray Diffractometer (Cambridge, United Kingdom) with a copper anode with an X-ray wavelength of 1.5418 Å. The measured angles (2θ) were scanned from 10° to 75° in 30 min; at a fixed divergence angle of 0.2°. The PDF database was used for phase identification. The average crystallite sizes were calculated according to the Scherrer equation [34] assuming spherical crystals (K = 0.9) using the diffraction peak between 2θ = 45–50°.

In situ powder XRD experiments were carried out at BM31 of the Swiss-Norwegian beam lines (SNBL) at the European Synchrotron Radiation Facility (ESRF). Catalyst sample (30mg, sieve fraction 53–90 μm) was fixed between two quartz wool plugs in a quartz capillary of 1 mm internal diameter (bed length: 10 mm). The capillary was then mounted in a custom cell [35] and exposed to X-rays for diffraction measurements. The temperature of the capillary reactor was controlled by a calibrated hot air blower. Powder X-ray diffraction patterns were collected with a 2D plate detector (Mar-345) using monochromatic radiation of wavelength 0.49324Å. Note that is different from the Cu Kα wavelength, which is used for acquiring ex situ XRD patterns. The instrumental peak broadening, wavelength calibration, and detector distance corrections were performed using a NIST 660a LaB_6 standard. Mass flow controllers were used to feed NO, O_2 and He in to produce the desired gas-feed composition (15 Ncm^3/min; 1% NO, 6% O_2, He balance). XRD patterns were recorded in situ during the

pretreatment step (flowing 15 Ncm^3/min of 6% O_2/He by heating at 10 °C/min from ambient to 500 °C and holding for 1 hr) and steady state NO oxidation (1%NO, 6% O_2 and balance He) at 350 °C for 2 h. A lower concentration of NO (1%) was used for the in situ studies due to experimental constraints at the beamline.

The morphological analysis of as-synthesized perovskites was performed by using an in-lens cold field emission electron microscope FE-S(T)EM, (Hitachi S-5500) in scanning electron microscopy (SEM) mode.

Temperature programmed reduction by H_2 was performed with an Altamira BenchCAT Hybrid 1000 HP (Pittsburgh, PA, USA). The samples (100 mg) were pretreated in 50 Ncm^3/min flow of Ar at 150 °C for 30 min, with a heating rate of 10 °C. TPR was conducted by heating at a rate of 5 °C/min from 50 to 850 °C with a 50 Ncm^3/min flow of 10% H_2/Ar.

3.3. Catalyst Activity Testing

Details of the reactor and experimental setup can be found in our previous publication [5]. Briefly, the activity of the catalysts was measured in a vertical stainless steel tubular reactor (internal diameter = 9.7 mm) operated at atmospheric pressure. The temperature was measured and controlled by a thermocouple, protected by a stainless steel jacket, inserted into the catalyst bed. A MKS MultiGas 2030-HS FTIR Gas Analyzer (path length 5.11 m, Cheshire, United Kingdom), calibrated at 1 bar and 191°C was used to analyze the composition of NO and NO_2 in the product stream.

For activity measurements, 0.5 g of catalyst diluted with 2.75 g SiC was loaded into the reactor and held in place by quartz wool plugs. Prior to the activity tests, the catalysts were pretreated at 500 °C for 1 h in 200 Ncm^3/min flow of 10% O_2/Ar and subsequently cooled down in inert argon atmosphere. The activity of the catalysts was investigated by heating from 150 to 450 °C at a rate of 5 °C/min under a flow of 200 Ncm^3/min of feed gas (10% NO, 6% O_2 in balance Ar).

Conversion of NO to NO_2 was calculated by the following equation:

$$\text{NO conversion} = \alpha \times [NO_2]_{outlet}/[NO]_{inlet} \tag{2}$$

where $[NO]_{inlet}$ and $[NO_2]_{outlet}$ are concentrations of NO at inlet and NO_2 at the outlet of the reactor. Volume changes arising from the reaction is taken into account by the constant "α" [36] where $\alpha = 0.99$. The closure of nitrogen balance across the reactor (99.5–100%) confirmed that all nitrogen is present as NO and NO_2. Comparison of catalyst activity is performed at 350 °C where the reaction is in the kinetic regime, away from equilibrium. The reaction rate (r_{NO}) calculations were performed by subtracting the homogeneous gas phase conversion of NO; hence, reflecting only the activity provided by the catalyst.

4. Conclusions

A series of lanthanum-based perovskites have been investigated for oxidation of NO using a feed containing 10% NO and 6% O_2, thus partially simulating nitric acid plant conditions. Among the undoped perovskites, the NO oxidation activity follows the order $LaCoO_3$ > $LaNiO_3$ > $LaMnO_3$. A significant increase in NO oxidation activity was achieved by partial substitution of cobalt in $LaCoO_3$ with 25 mol% of either nickel or manganese. Further increase in the degree of Co substitution had a negative impact on activity.

From this work, perovskites are shown to be promising catalysts for oxidizing NO to NO_2 at conditions representative of nitric acid plant operation. Low cost, ease of production and significant catalytic activity make perovskites attractive candidates as alternatives to noble metal catalysts.

Author Contributions: Conceptualization, A.u.R.S., D.W., B.C.E., R.L. and M.R.; methodology, A.S., S.M.H.; formal analysis, A.u.R.S., S.M.H., S.K.R. and M.Z.; investigation, A.u.R.S., S.M.H., S.K.R. and M.Z.; writing—original draft preparation, A.u.R.S.; writing—review and editing, S.M.H., S.K.R, M.Z., B.C.E., R.L, D.W. and M.R.; visualization, A.u.R.S.; supervision, B.C.E., R.L. and M.R.; project administration, M.R.; funding acquisition, B.C.E., R.L., D.W. and M.R.

Conflicts of Interest: The authors declare no conflict of interest.

References

1. Baulch, D.; Drysdale, D.; Horne, D. *Homogeneous Gas Phase Reactions of the H_2-N_2-O_2 System*; CRC Press: Boca Raton, FL, USA, 1973; pp. 285–300.

2. Honti, G. *The Nitrogen Industry*; Akademiai Kiado: Budapest, Hungary, 1976; pp. 400–413.

3. Klingelhoefer, W.C. Nitric Oxide Oxidation. US2115173 A, 26 April 1938.

4. Grande, C.A.; Andreassen, K.A.; Cavka, J.H.; Waller, D.; Lorentsen, O.-A.; Øien, H.; Zander, H.-J.; Poulston, S.; García, S.; Modeshia, D. Process intensification in nitric acid plants by catalytic oxidation of nitric oxide. *Ind. Eng. Chem. Res.* **2018**, *57*, 10180–10186. [CrossRef]

5. Salman, A.u.R.; Enger, B.C.; Auvray, X.; Lødeng, R.; Menon, M.; Waller, D.; Rønning, M. Catalytic oxidation of NO to NO_2 for nitric acid production over a Pt/Al_2O_3 catalyst. *Appl. Catal. A Gen.* **2018**, *564*, 142–146. [CrossRef]

6. Russell, A.; Epling, W.S. Diesel oxidation catalysts. *Catal. Rev.* **2011**, *53*, 337–423. [CrossRef]

7. Hong, Z.; Wang, Z.; Li, X. Catalytic oxidation of nitric oxide (NO) over different catalysts: An overview. *Catal. Sci. Technol.* **2017**, *7*, 3440–3452. [CrossRef]

8. Auvray, X.; Olsson, L. Stability and activity of Pd-, Pt- and Pd–Pt catalysts supported on alumina for NO oxidation. *Appl. Catal. B Environ.* **2015**, *168–169*, 342–352. [CrossRef]

9. Auvray, X.; Pingel, T.; Olsson, E.; Olsson, L. The effect gas composition during thermal aging on the dispersion and NO oxidation activity over Pt/Al_2O_3 catalysts. *Appl. Catal. B Environ.* **2013**, *129*, 517–527. [CrossRef]

10. Després, J.; Elsener, M.; Koebel, M.; Kröcher, O.; Schnyder, B.; Wokaun, A. Catalytic oxidation of nitrogen monoxide over Pt/SiO_2. *Appl. Catal. B Environ.* **2004**, *50*, 73–82. [CrossRef]

11. Zhu, J.; Thomas, A. Perovskite-type mixed oxides as catalytic material for NO removal. *Appl. Catal. B Environ.* **2009**, *92*, 225–233. [CrossRef]

12. Onrubia, J.A.; Pereda-Ayo, B.; De-La-Torre, U.; González-Velasco, J.R. Key factors in Sr-doped $LaBO_3$ (B=Co or Mn) perovskites for NO oxidation in efficient diesel exhaust purification. *Appl. Catal. B Environ.* **2017**, *213*, 198–210. [CrossRef]

13. Zhong, S.; Sun, Y.; Xin, H.; Yang, C.; Chen, L.; Li, X. NO oxidation over Ni–Co perovskite catalysts. *Chem. Eng. J.* **2015**, *275*, 351–356. [CrossRef]

14. Kim, C.H.; Qi, G.; Dahlberg, K.; Li, W. Strontium-doped perovskites rival platinum catalysts for treating NO_x in simulated diesel exhaust. *Science* **2010**, *327*, 1624–1627. [CrossRef]

15. Wen, Y.; Zhang, C.; He, H.; Yu, Y.; Teraoka, Y. Catalytic oxidation of nitrogen monoxide over $La_{1-x}Ce_xCoO_3$ perovskites. *Catal. Today* **2007**, *126*, 400–405. [CrossRef]

16. Wang, J.; Su, Y.; Wang, X.; Chen, J.; Zhao, Z.; Shen, M. The effect of partial substitution of Co in $LaMnO_3$ synthesized by sol–gel methods for NO oxidation. *Catal. Commun.* **2012**, *25*, 106–109. [CrossRef]

17. Taguchi, H.; Matsu-ura, S.-i.; Nagao, M.; Choso, T.; Tabata, K. Synthesis of $LaMnO_{3+\delta}$ by firing gels using citric acid. *J. Solid State Chem.* **1997**, *129*, 60–65. [CrossRef]

18. Taguchi, H.; Yamada, S.; Nagao, M.; Ichikawa, Y.; Tabata, K. Surface characterization of $LaCoO_3$ synthesized using citric acid. *Mater. Res. Bull.* **2002**, *37*, 69–76. [CrossRef]

19. Alifanti, M.; Auer, R.; Kirchnerova, J.; Thyrion, F.; Grange, P.; Delmon, B. Activity in methane combustion and sensitivity to sulfur poisoning of $La_{1-x}Ce_xMn_{1-y}Co_yO_3$ perovskite oxides. *Appl. Catal. B Environ.* **2003**, *41*, 71–81. [CrossRef]

20. Silva, C.R.B.; da Conceição, L.; Ribeiro, N.F.P.; Souza, M.M.V.M. Partial oxidation of methane over Ni–Co perovskite catalysts. *Catal. Commun.* **2011**, *12*, 665–668. [CrossRef]

21. Ghiasi, M.; Delgado-Jaime, M.U.; Malekzadeh, A.; Wang, R.-P.; Miedema, P.S.; Beye, M.; de Groot, F.M.F. Mn and Co charge and spin evolutions in $LaMn_{1-x}Co_xO_3$ nanoparticles. *J. Phys. Chem. C* **2016**, *120*, 8167–8174. [CrossRef]

22. Chen, J.; Shen, M.; Wang, X.; Qi, G.; Wang, J.; Li, W. The influence of nonstoichiometry on LaMnO$_3$ perovskite for catalytic NO oxidation. *Appl. Catal. B Environ.* **2013**, *134–135*, 251–257. [CrossRef]

23. Pecchi, G.; Campos, C.; Peña, O.; Cadus, L.E. Structural, magnetic and catalytic properties of perovskite-type mixed oxides LaMn$_{1−y}$Co$_y$O$_3$ (y = 0.0, 0.1, 0.3, 0.5, 0.7, 0.9, 1.0). *J. Mol. Catal. A Chem.* **2008**, *282*, 158–166. [CrossRef]

24. Rakshit, S.; Gopalakrishnan, P.S. Oxygen nonstoichiometry and its effect on the structure of LaNiO$_3$. *J. Solid State Chem.* **1994**, *110*, 28–31. [CrossRef]

25. Zhou, C.; Feng, Z.; Zhang, Y.; Hu, L.; Chen, R.; Shan, B.; Yin, H.; Wang, W.G.; Huang, A. Enhanced catalytic activity for NO oxidation over Ba doped LaCoO$_3$ catalyst. *RSC Adv.* **2015**, *5*, 28054–28059. [CrossRef]

26. Qi, G.; Li, W. Pt-free, LaMnO$_3$ based lean NO$_x$ trap catalysts. *Catal. Today* **2012**, *184*, 72–77. [CrossRef]

27. Batiot-Dupeyrat, C.; Valderrama, G.; Meneses, A.; Martinez, F.; Barrault, J.; Tatibouët, J.M. Pulse study of Co$_2$ reforming of methane over LaNiO$_3$. *Appl. Catal. A Gen.* **2003**, *248*, 143–151. [CrossRef]

28. Benard, S.; Retailleau, L.; Gaillard, F.; Vernoux, P.; Giroir-Fendler, A. Supported platinum catalysts for nitrogen oxide sensors. *Appl. Catal. B Environ.* **2005**, *55*, 11–21. [CrossRef]

29. Mulla, S.S.; Chen, N.; Cumaranatunge, L.; Blau, G.E.; Zemlyanov, D.Y.; Delgass, W.N.; Epling, W.S.; Ribeiro, F.H. Reaction of NO and O$_2$ to NO$_2$ on Pt: Kinetics and catalyst deactivation. *J. Catal.* **2006**, *241*, 389–399. [CrossRef]

30. Schmitz, P.J.; Kudla, R.J.; Drews, A.R.; Chen, A.E.; Lowe-Ma, C.K.; McCabe, R.W.; Schneider, W.F.; Goralski, C.T. NO oxidation over supported Pt: Impact of precursor, support, loading, and processing conditions evaluated via high throughput experimentation. *Appl. Catal. B Environ.* **2006**, *67*, 246–256. [CrossRef]

31. Wang, H.; Chen, H.; Wang, Y.; Lyu, Y.-K. Performance and mechanism comparison of manganese oxides at different valence states for catalytic oxidation of NO. *Chem. Eng. J.* **2019**, *361*, 1161–1172. [CrossRef]

32. Ivanova, S.; Senyshyn, A.; Zhecheva, E.; Tenchev, K.; Stoyanova, R.; Fuess, H. Crystal structure, microstructure and reducibility of LaNi$_x$Co$_{1−x}$O$_3$ and LaFe$_x$Co$_{1−x}$O$_3$ perovskites (0 <x ≤ 0.5). *J. Solid State Chem.* **2010**, *183*, 940–950.

33. Brunauer, S.; Emmett, P.H.; Teller, E. Adsorption of gases in multimolecular layers. *JACS* **1938**, *60*, 309–319. [CrossRef]

34. Scherrer, P. Bestimmung der größe und der inneren struktur von kolloidteilchen mittels röntgenstrahlen. *Nachr. Ges. Wiss. Gött. Math. Phys. Kl.* **1918**, *1918*, 98–100.

35. Tsakoumis, N.E.; Voronov, A.; Rønning, M.; Beek, W.v.; Borg, Ø.; Rytter, E.; Holmen, A. Fischer–tropsch synthesis: An XAS/XRPD combined in situ study from catalyst activation to deactivation. *J. Catal.* **2012**, *291*, 138–148. [CrossRef]

36. Fogler, H. *Elements of Chemical Reaction Engineering*; Prentice-Hall of India: New Delhi, India, 2006; p. 92.